PROCEEDINGS OF SCIENCE

Hard probes at intermediate energies (including fixed-target programs)

Rongrong Ma[a,*]

[a] *Brookhaven National Laboratory,*
PO Box 5000, Upton, NY 11973, USA

E-mail: marr@bnl.gov

This contribution overviews recent progresses on utilizing hard probes (particles of high transverse momentum (p_{T}) or large mass) to explore a variety of topics in p+A and A+A collisions with center-of-mass energies below 200 GeV. This includes: *i)* search for the intrinsic charm in nucleons; *ii)* measurements of high-p_{T} hadrons, electrons from heavy favor hadron decay, thermal dilepton and J/ψ at various beam energies; *iii)* theoretical perspective on probing collision dynamics with photons. An outlook to future measurements and programs, including phase-II of the beam energy scan program at RHIC and the NA60+ experiment proposed at SPS, is also given.

HardProbes2023
26-31 March 2023
Aschaffenburg, Germany

*Speaker

PoS(HardProbes2023)031

1. Search for the intrinsic charm

Quantum ChromoDynamics (QCD) describes the proton as three valence quarks (two up quarks and one down quark) bound by gluons. A nonperturbative charm contribution to the proton wavefunction, known as the intrinsic charm, was predicted in early 1980s [1]. Since then, numerous efforts have been made experimentally to search for the evidence of intrinsic charm by measuring charm hadron production, such as J/ψ and D^0 mesons. Recently, a combination of theoretical calculations with a wealth of experimental data suggested the existence of intrinsic charm at a 3-standard-deviation level [2]. But further confirmation is still needed.

The left panel of Fig. 1 shows the J/ψ cross section per nucleon as a function of center-of-mass rapidity in fixed-target p+Ne collisions at the center-of-mass energy ($\sqrt{s_{\rm NN}}$) of 68.5 GeV, measured by the LHCb experiment [3]. The J/ψ cross section decreases from middle to large rapidity, as expected. These results are compared to theoretical calculations without (red hatched band) and with 1% (green hatched band) intrinsic charm contribution to the proton content [4]. Within uncertainties, both calculations are consistent with experimental data. It is worth noting that the difference between with and without intrinsic charm contribution is actually even smaller than the theoretical uncertainty within the measured kinematic range, making it extremely challenging to distinguish the two scenarios.

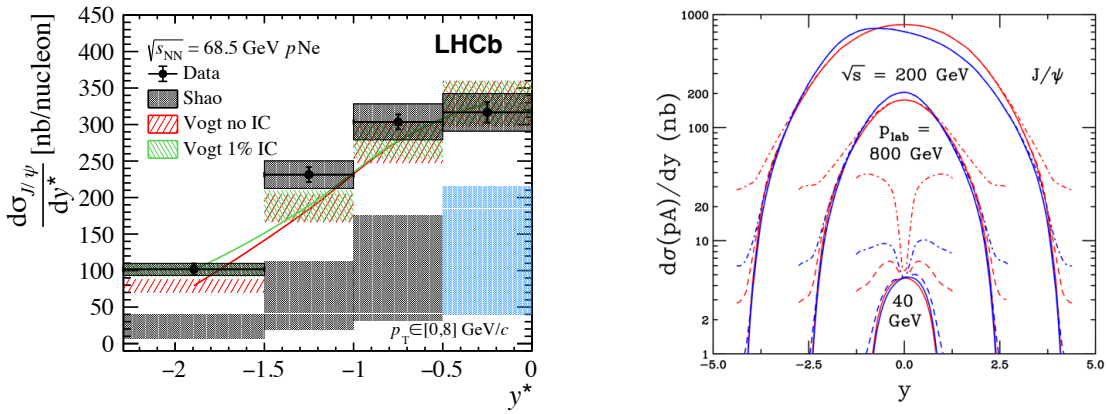

Figure 1: Left: J/ψ cross section per nucleon as a function of rapidity in center-of-mass frame in p+Ne collisions at $\sqrt{s_{\rm NN}}$ = 68.5 GeV by the LHCb experiment [3]. Theoretical calculations without (red) and with 1% intrinsic charm (green) [4] are shown for comparison. Right: NLO pQCD calculations of the rapidity dependence of the J/ψ cross section in p+p (red) and p+Pb (blue) collisions at various collision energies [5]. Solid, dashed and dot-dashed lines correspond to 0%, 0.1% and 1% intrinsic charm in the proton, respectively.

To provide further guidance on where to search for the intrinsic charm, pQCD calculations at Next-to-Leading Order (NLO) are performed for a five-quark Fock state ($|uudc\bar{c}\rangle$) in the proton wavefunction [5] . The resulting J/ψ cross sections as a function of center-of-mass rapidity are shown in the right panel of Fig. 1 in p+p (red) and p+Pb (blue) collisions at three collision energies, $\sqrt{s_{\rm NN}}$ = 200, 38.8, and 8.8 GeV. The later two correspond to incident beam energies of 800 and 40 GeV, respectively, in a fixed-target setup. Calculations for 0%, 0.1% and 1% intrinsic charm contribution are illustrated by solid, dashed and dot-dashed lines in the figure. The effect of intrinsic

charm at midrapidity ($|y| < 1$) deceases with increasing beam energy since intrinsic charm quarks are expected to carry a large fraction of the proton momentum and thus should manifest themselves at larger rapidities for higher energies. This motivates the search to concentrate at low energy for an experiment covering midrapidity region. As shown in Fig. 1, right panel, the J/ψ cross section is predicted to increase by about 25 fold at $y \sim 1$ in p+p collisions at $\sqrt{s} = 8.8$ GeV if a proton contains 1% of intrinsic charm. While the effect for p+Pb collisions is significantly smaller compared to p+p due to nuclear attenuation, it is still desirable to measure the ratio of J/ψ cross section in p+p and p+Pb collisions to search for intrinsic charm since both experimental and theoretical uncertainties cancel to a large extent for the ratio.

2. Measurements at RHIC beam energy scan

Understanding the phase diagram of the QCD matter under different conditions of temperature (T) and baryon chemical potential (μ_B) is a key objective of the heavy-ion physics. To facilitate this exploration, two campaigns of Beam Energy Scan (BES) were conducted at RHIC in 2010-2014 and 2017-2021, during which Au+Au collisions with energies ranging between 3 to 62.4 GeV were delivered. This section presents measurements of thermal photons and dielectrons, hadrons of high transverse momenta (p_T), heavy-flavor electrons and J/ψ with BES data.

Throughout the evolution of the Quark-Gluon Plasma (QGP), a deconfined QCD matter created in heavy-ion collisions, thermal photons and dileptons are emitted continuously from the system, and their properties are closely related to the medium temperature. For example, high-p_T photons and large-mass dileptons are radiated at the early stage of the evolution when the system temperature is high. Therefore, their spectra can serve as a thermometer to the QGP. In the left panel of Fig. 2, the effective temperature ($T_{\rm eff}$) in different p_T ranges of the thermal photon spectra is shown as a function of beam energy [6, 7]. $T_{\rm eff}$ is extracted by fitting the thermal photon p_T spectra with an

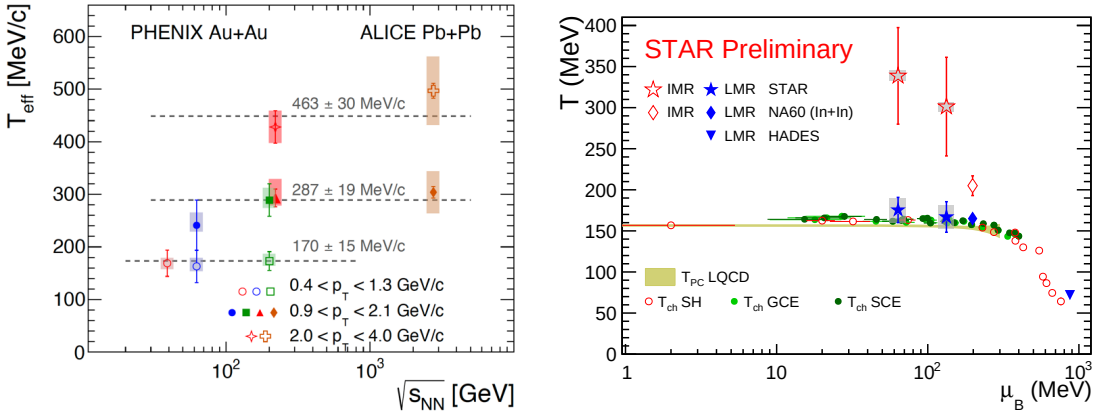

Figure 2: Left: effective temperature, extracted from p_T spectra of thermal photons as the inverse slope parameter, as a function of beam energy [6, 7]. Right: medium temperature as a function of baryon chemical potential extracted from invariant mass distributions of dilepton production measured by STAR (open star) and NA60 (open diamond) [8, 9]. They are compared to theoretical calculations of pseudocritical ($T_{\rm pc}$) [10] and chemical freeze-out temperatures ($T_{\rm ch}$) [11].

exponential function, in which $T_{\rm eff}$ is the inverse of the slope parameter. As expected, $T_{\rm eff}$ increases

with increasing p_T. In the highest p_T range of 2 - 4 GeV/c, there is a hint of increasing T_{eff} with collision energy, suggesting a hotter QGP created at higher energy. However, it is important to point out that inferring the QGP temperature from T_{eff} needs to take into account the effect of radial flow on the photons, the so-called "blue shift" effect, which is model dependent and not well established. To overcome this difficulty, invariant mass distribution of thermal dilepton production can be used, which does not suffer from the radial flow effect. The STAR collaboration measured the dielectron production in the invariant mass range of $1 < M < 3$ GeV/c^2, and extracted the slope parameter, a true measure of the average QGP temperature under which those dielectrons are emitted. The results for Au+Au collisions at $\sqrt{s_{NN}}$ = 27 and 54.4 GeV are shown in the right panel of Fig. 2 as open stars. They are seen to be consistent higher than the pseudocritical [10] or chemical freeze-out temperature [11] at the phase boundary of partonic and hadronic matter. Such a temperature is extracted similarly based on the dimuon invariant mass spectrum measured by the NA60 collaboration [8, 9] in In+In collisions at $\sqrt{s_{NN}}$ = 17.3 GeV. It is shown as the open diamond in Fig. 2, and seems to be lower than the temperature at higher RHIC energies.

Suppression of high-p_T hadrons due to jet quenching is another signature of the QGP formation, which can be used to signify the onset of deconfinement using BES data. On the other hand, the

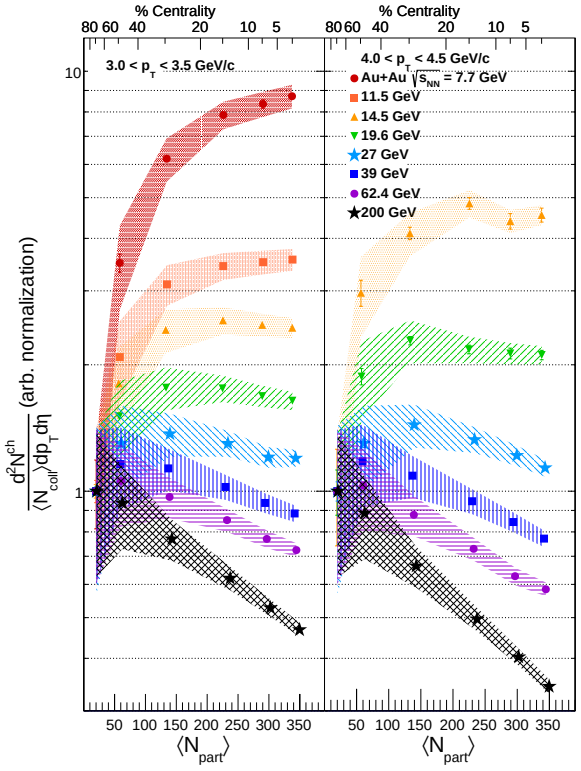

Figure 3: High-p_T charged particle yield, scaled by N_{coll}, as a function centrality measured in Au+Au collisions at $\sqrt{s_{NN}}$ = 7.7 to 200 GeV [12]. The left panel is for the range of $3.0 < p_T < 3.5$ GeV/c, while the right panel is for $4.0 < p_T < 4.5$ GeV/c.

Cronin effect, which could arise from k_T broadening, can enhance the production of high-p_T hadrons which acts against the jet quenching signal. Since both effects increase with collision centrality, it is instructive to study the centrality dependence of high-p_T hadron production. Figure 3 shows the

yields of charged hadrons with $3.0 < p_T < 3.5$ GeV/c (left) $4.0 < p_T < 4.5$ GeV/c (right), scaled by the number of binary collisions (N_{coll}) to take out the trivial geometric effect, as a function of centrality represented by the number of participating nucleons (N_{part}). Different sets of data points correspond to different collision energies. At $\sqrt{s_{NN}}$ = 14.5 GeV and above, the high-p_T hadron yields decrease in the 0-5% most central collisions compared to those in 5-10% centrality, indicating the dominance of the jet quenching effect and thus the creation of the QGP. On the other hand, such a yield increases monotonically with centrality for $\sqrt{s_{NN}}$ = 11.5 GeV and below, which suggests the dominance of the Cronin effect. However, creation of the QGP could not be ruled out at these energies.

Another type of hard probes widely used to probe the properties of the QGP is the heavy flavor quarks. Due to their large masses, heavy flavor quarks are predominantly produced at the early stage of a heavy-ion collision. They subsequently traverse the medium throughout its entire evolution, and encode the QGP information via strong interactions. The left panel of Fig. 4 shows the elliptic flow (v_2) of electrons from heavy flavor hadron decays (HFE) as a function of collision energy [13] as filled circles. The measured v_2 value at 54.4 GeV is consistent with those at 200 GeV and 2.76 TeV within uncertainties, indicating that not only a hot, dense medium is created at 54.4 GeV, but also the strength of the medium interaction with heavy quarks seems compatible at 54.4 GeV and above. At 27 GeV, the HFE v_2 is consistent with 0, but the uncertainty is quite large. The results are compared with those for π and ϕ mesons at the same $\langle k_T \rangle = \langle \sqrt{p_T^2 + m_0^2} - m_0 \rangle$, where m_0 is the particle's rest mass, and the parent D^0 $\langle k_T \rangle$ is used for HFE. A hint of mass ordering is seen that heavier particle's v_2 drops faster with decreasing energy than that of lighter particles, which could potentially be due to that the medium created at low energies does not live long enough or its density is high enough to thermalize heavy quarks. The right panel of Fig. 4 shows inclusive J/ψ R_{AA} as

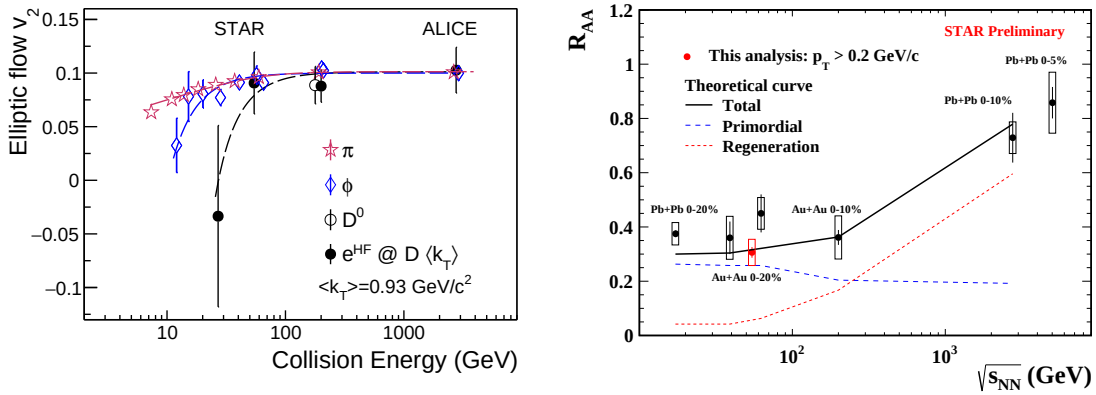

Figure 4: Collision energy dependence of heavy-flavor electron v_2 (left) [13] and J/ψ R_{AA} (right) [14–18].

a function of collision energy [14–18]. At $\sqrt{s_{NN}} \leq 200$ GeV, the level of suppression has a weak dependence on collision energy. A transport model calculation (solid line), including the interplay of Cold Nuclear Matter (CNM) effect, dissociation and regeneration, can qualitatively describe the observed trend [19]. As indicated by the blue dashed line, the effect of suppression arising from CNM effect and dissociation increases with collision energy due to the creation of a hotter and denser medium, which, however, is compensated by the increased regeneration contribution that

also increases with collision energy thanks to the enhanced charm quark production cross section. At the LHC energies, the regeneration contribution completely overtakes the suppression effect.

3. Utilize thermal photons to probe collision dynamics

Theoretical descriptions of heavy-ion collisions at BES energies are essential for interpreting the results presented in Sec. 2, from which one can extract QGP properties and map out the QCD diagram. One key difference between heavy-ion collisions at low energies and those at top RHIC and LHC energies is that incoming nuclei are not longer Lorentz-contracted as pancakes. Instead, they have a finite extend along the longitudinal direction and expected to take longer to collide with each other. Consequently, the kinetic energy of the incoming nuclei will be deposited dynamically, and the system's temperature turns on relatively slowly before it decreases due to expansion [20]. The predicted yield (left) and v_2 (right) for thermal photons radiated throughout the system's evolution based on the dynamical energy deposition are shown in Fig. 5 as black solid lines. They are

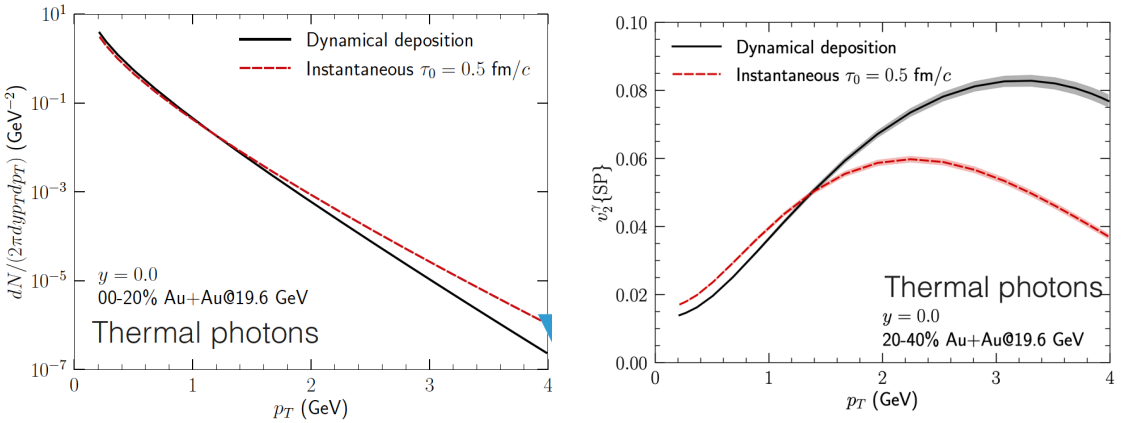

Figure 5: Predicted thermal photon yield (left) and v_2 (right) as a function of p_T for two scenarios of collision dynamics: dynamical deposition of incoming nuclei's kinetic energy into vacuum vs. instantaneous deposition at an initial time of τ_0 = 0.5 fm/c [20].

compared to the predictions assuming all the energies are deposited into vacuum instantaneously at τ_0 = 0.5 fm/c (red dashed lines), and the medium's temperature reaches its peak value also instantaneously. Due to the turn-on of the medium temperature for dynamical deposition at the initial stage, high-p_T photons emitted at this stage are predicted to be less compared to instantaneous deposition, while the expected photon v_2 is larger at high p_T due to the larger contribution from later stages when the anisotropic flow is more developed. Therefore, measurements of thermal photon yield and v_2 at BES energies can shed light on the process of energy deposition at the first instances of the collision.

4. Summary and outlook

In this contribution, an overview of recent measurements on hard probes (heavy flavor, high-p_T hadrons, dileptons) is presented, focusing on collision energies below the top RHIC energy of 200 GeV and including fixed-target programs. The search for the intrinsic charm in the proton

wavefunction continues as it has only been established at the 3-standard-deviation level. Theoretical calculations suggest that it is more favorable to conduct such searches at low energy ($\sim$ 10 GeV). On the other hand, comprehensive studies of QGP formation and its properties have been carried out with the beam energy scan programs at RHIC. It seems that the QGP is formed in central collisions at energies of 14.5 GeV and above, and at 54.4 GeV and above the created medium can potentially thermalize charm quarks. In addition, measurements of thermal photons at low energies will help understand the initial collision dynamics.

Going into the future, to fully exploit the potential of using hard probes measurements to study QGP's properties and QCD phase diagram, it is vital to improve the precision of those measurements. The recently recorded data sets from BES phase-II by the STAR experiment, as well as planned high interaction rate experiments in the near future, as illustrated in Fig. 6, will contribute to that. Moreover, understanding the CNM effects, which are usually quantified using p+A collisions, also plays a vital role in interpreting heavy-ion results, which deserve great attention. A dedicated experiment, called NA60+ [21], has been proposed to be built at SPS. It covers the energy range of 6 - 17.3 GeV, and is designed in particular to precisely measure thermal dimuon production and medium modifications to J/ψ and D^0. This energy range is also suitable for intrinsic charm search as guided by theoretical calculations. p+A collisions corresponding to the planned A+A running will also be recorded to provide the baseline without hot medium creation but with nuclei present in the collisions. The proposed running time for NA60+ is 2029 and beyond.

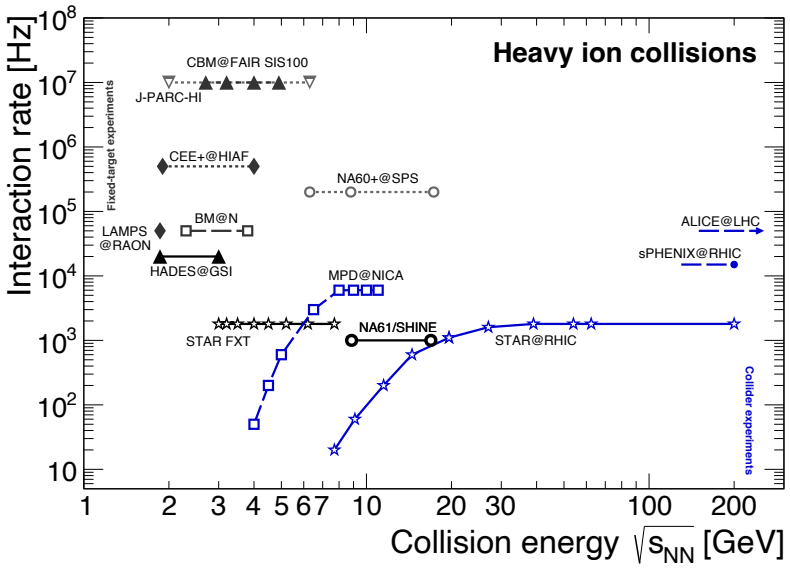

Figure 6: Landscape of heavy-ion experiments, in terms of collision energy and collision rate, currently running and planned for the future [21, 22].

In conclusion, recorded data on tape and planned heavy-ion experiments at intermediate energies will allow continuing investigations of QCD matter with large baryon chemical potentials, and shed new light on the QCD phase diagram.

References

[1] S.J. Brodsky, P. Hoyer, C. Peterson and N. Sakai, *The Intrinsic Charm of the Proton*, *Phys. Lett. B* **93** (1980) 451.

[2] NNPDF collaboration, *Evidence for intrinsic charm quarks in the proton*, *Nature* **608** (2022) 483 [2208.08372].

[3] LHCB collaboration, *Charmonium production in pNe collisions at* $\sqrt{s_{\rm NN}}$ = 68.5 *GeV*, 2211.11645.

[4] R. Vogt, *Limits on Intrinsic Charm Production from the SeaQuest Experiment*, *Phys. Rev. C* **103** (2021) 035204 [2101.02858].

[5] R. Vogt, *Energy dependence of intrinsic charm production: Determining the best energy for observation*, *Phys. Rev. C* **106** (2022) 025201 [2207.04347].

[6] PHENIX collaboration, *Low-pT direct-photon production in Au+Au collisions at sNN=39 and 62.4 GeV*, *Phys. Rev. C* **107** (2023) 024914 [2203.12354].

[7] PHENIX collaboration, *Nonprompt direct-photon production in Au+Au collisions at* $\sqrt{s_{NN}}$ = 200 *GeV*, 2203.17187.

[8] NA60 collaboration, *Evidence for the production of thermal-like muon pairs with masses above 1-GeV/c**2 in 158-A-GeV Indium-Indium Collisions*, *Eur. Phys. J. C* **59** (2009) 607 [0810.3204].

[9] NA60 collaboration, *Thermal Dileptons from Hot and Dense Strongly Interacting Matter*, *AIP Conf. Proc.* **1322** (2010) 1 [1011.0615].

[10] HotQCD collaboration, *Chiral crossover in QCD at zero and non-zero chemical potentials*, *Phys. Lett. B* **795** (2019) 15 [1812.08235].

[11] A. Andronic, P. Braun-Munzinger, K. Redlich and J. Stachel, *Decoding the phase structure of QCD via particle production at high energy*, *Nature* **561** (2018) 321 [1710.09425].

[12] STAR collaboration, *Beam Energy Dependence of Jet-Quenching Effects in Au+Au Collisions at* $\sqrt{s_{\rm NN}}$ *= 7.7, 11.5, 14.5, 19.6, 27, 39, and 62.4 GeV*, *Phys. Rev. Lett.* **121** (2018) 032301 [1707.01988].

[13] STAR collaboration, *Elliptic Flow of Heavy-Flavor Decay Electrons in Au+Au Collisions at* $\sqrt{s_{\rm NN}}$ *= 27 and 54.4 GeV at RHIC*, 2303.03546.

[14] NA50 collaboration, *Evidence for deconfinement of quarks and gluons from the J / psi suppression pattern measured in Pb + Pb collisions at the CERN SPS*, *Phys. Lett. B* **477** (2000) 28.

[15] STAR collaboration, *Energy dependence of* J/ψ *production in Au+Au collisions at* $\sqrt{s_{NN}}$ = *39, 62.4 and 200 GeV*, *Phys. Lett. B* **771** (2017) 13 [1607.07517].

[16] STAR collaboration, *Measurement of inclusive J/ψ suppression in Au+Au collisions at $\sqrt{s_{NN}} = 200$ GeV through the dimuon channel at STAR*, *Phys. Lett. B* **797** (2019) 134917 [1905.13669].

[17] ALICE collaboration, *Centrality, rapidity and transverse momentum dependence of J/ψ suppression in Pb-Pb collisions at $\sqrt{s_{\rm NN}}$=2.76 TeV*, *Phys. Lett. B* **734** (2014) 314 [1311.0214].

[18] ALICE collaboration, *Quarkonium measurements in nucleus-nucleus collisions with ALICE*, *Nucl. Phys. A* **1005** (2021) 121769 [2001.11925].

[19] X. Zhao and R. Rapp, *Charmonium in Medium: From Correlators to Experiment*, *Phys. Rev. C* **82** (2010) 064905 [1008.5328].

[20] C. Shen and B. Schenke, *Dynamical initialization and hydrodynamic modeling of relativistic heavy-ion collisions*, *Nucl. Phys. A* **982** (2019) 411 [1807.05141].

[21] NA60+ collaboration, *Letter of Intent: the NA60+ experiment*, 2212.14452.

[22] T. Galatyuk, *Future facilities for high μ_B physics*, *Nucl. Phys. A* **982** (2019) 163.